Electronic Supplementary Material (ESI) for Journal of Materials Chemistry C.
This journal is © The Royal Society of Chemistry 2018

Supplementary information

PPy/Cu_2O molecular imprinting composite film based visible light-responsive photoelectrochemical sensor for microcystin-LR

Junli Chen,[a]* Pan Gao,[b] Hai Wang,[a] Lifeng Han,[a] Yonghui Zhang,[a] Peiyuan Wang,[a] NengqinJia[b]*

[a]School of Materials and Chemical Engineering, Collaborative Innovation Center of Environmental Pollution Control and Ecological Restoration, Zhengzhou University of Light Industry, Zhengzhou 450001, PR China.

[b]*The Education Ministry Key Laboratory of Resource Chemistry, Shanghai Key Laboratory of Rare Earth Functional Materials, Department of Chemistry, Shanghai Normal University, Shanghai 200234, PR China*

*Corresponding Author. Tel/Fax: +86-371-8660 9676.

E-mail: chenjunli@zzuli.edu.cn,nqjia@shnu.edu.cn.

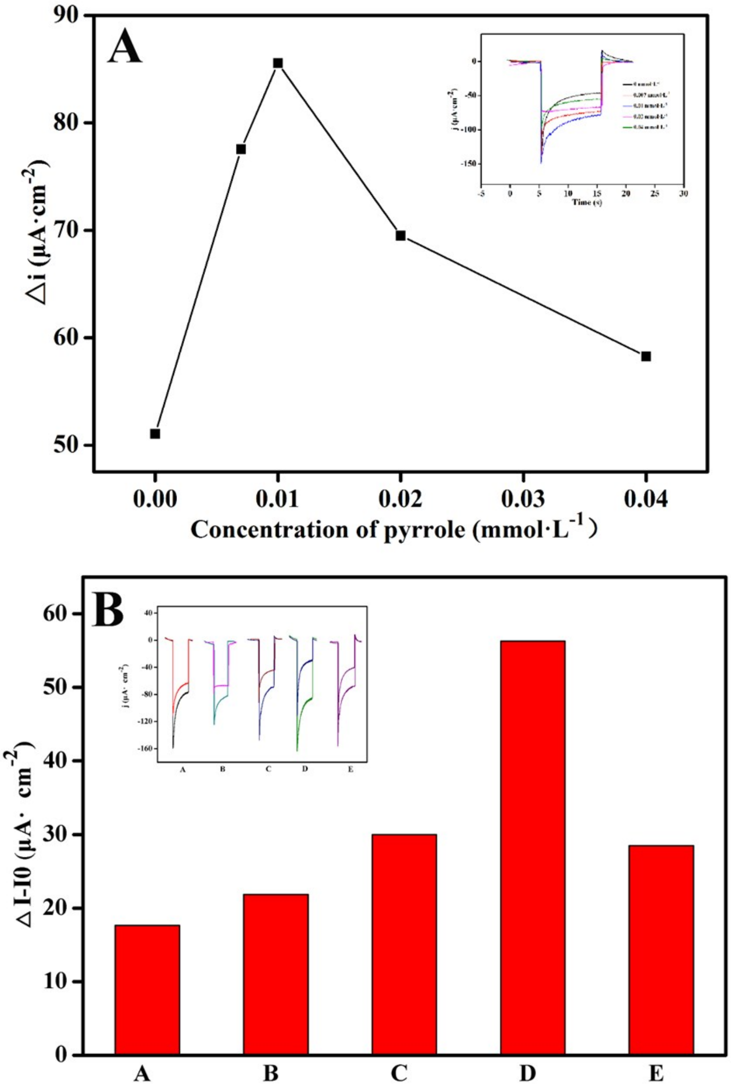

Fig. S1. (A) Effect of the concentration of pyrrole monomer on the photocurrent response. (B) Photocurrent responses of the PEC sensor fabricated using different proportions of monomers to template molecules. (from A to E: 10:0, 10:0.01, 10:0.4, 10:0.7, 10:1.4).

The photocurrent values of the PEC sensors were extensively affected by the concentration of pyrrole. As shown in Fig. S1A, the results indicated that the photocurrent value increased with the concentration of pyrrole and reached the maximum value about 87 μA·cm^{-2} when the pyrrole concentration was 0.01 mmol·L^{-1}. However, the concentration of pyrrole was enlarged further, the photocurrent value decreased. So the concentration of pyrrole equal to 0.01 mmol·L^{-1} was chosen for subsequent experiments. The performance of MIP was also affected by the molar ratio of monomers (pyrrole) to template molecules (MC-LR). In order to get the biggest photocurrent response of PEC sensor, MIP was synthesized using different proportions of monomers and template molecules. Fig. S1B showed the photocurrent responses of MIP sensor in PBS buffer solution and PBS buffer solution containing 1.0 μg·L MC-LR. It can be seen that the largest photocurrent response was obtained at the ratio of pyrrole to MC-LR equal to 10:0.7. Thus, the optimal experiment conditions were the phosphate-buffered solution (PBS) containing 0.1 mol·L-1 $LiClO_4$, 700 μg·L^{-1} MC-LR as template molecules and 0.01 mmol·L^{-1} pyrrole as functional monomers.

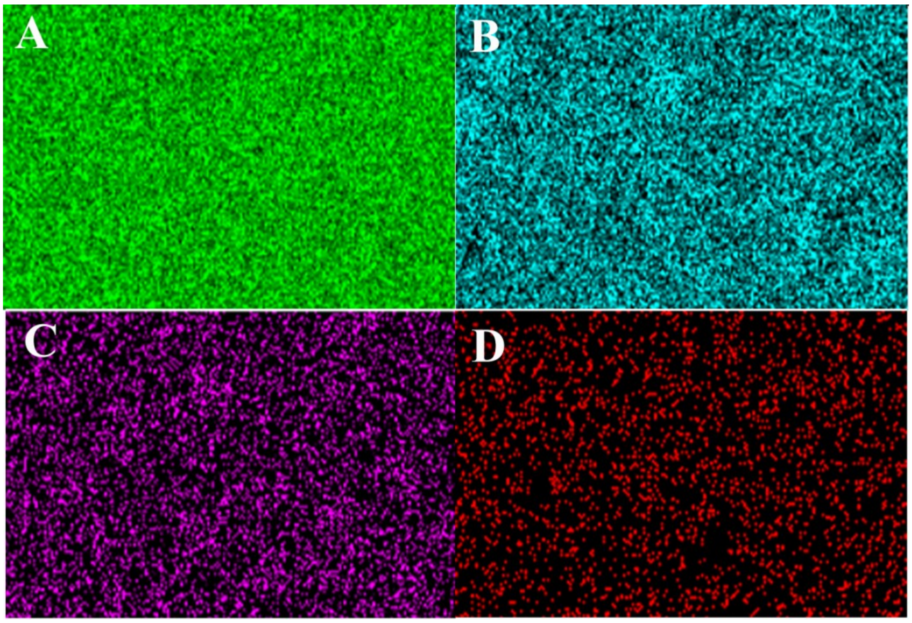

Fig. S2. Mapping images of individual atoms (A) Cu, (B) O, (C) C and (D) N on the MIP/Cu_2O/ITO electrode surface.

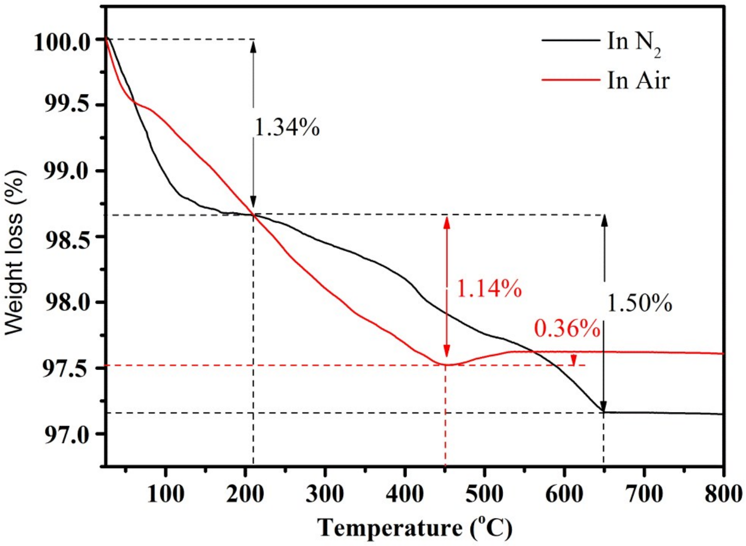

Fig. S3 TG curves of MIP/Cu_2O/ITO electrode.

The thermogravimetric analysis is applied to determine the content of PPy on MIP/Cu_2O/ITO electrode, and the results are shown in Fig. S3. The first weight loss was about 1.34% between 25 – 210 ^oC which could be ascribed to the physically and chemically adsorbed water for MIP/Cu_2O/ITO electrode measured in N_2 or air flow. The second weight loss between 210 – 650 ^oC was calculated as 1.50% for MIP/Cu_2O/ITO electrode treated in N_2 stream, which might be attributed to the decomposition of PPy.[1] However, the weight loss of the second stage in air flow between 210 – 450 ^oC was about 1.14%, and reduced about 0.36% compared with that in N_2 flow, which might be due to the full oxidation of PPy and partially oxidation of Cu_2O to CuO. Additionally, the third weight increment about 0.11% in air flow could be ascribed to the partially oxidation of Cu_2O to CuO. According to the TG results, the PPy content of MIP/Cu_2O/ITO electrode was 1.50%.

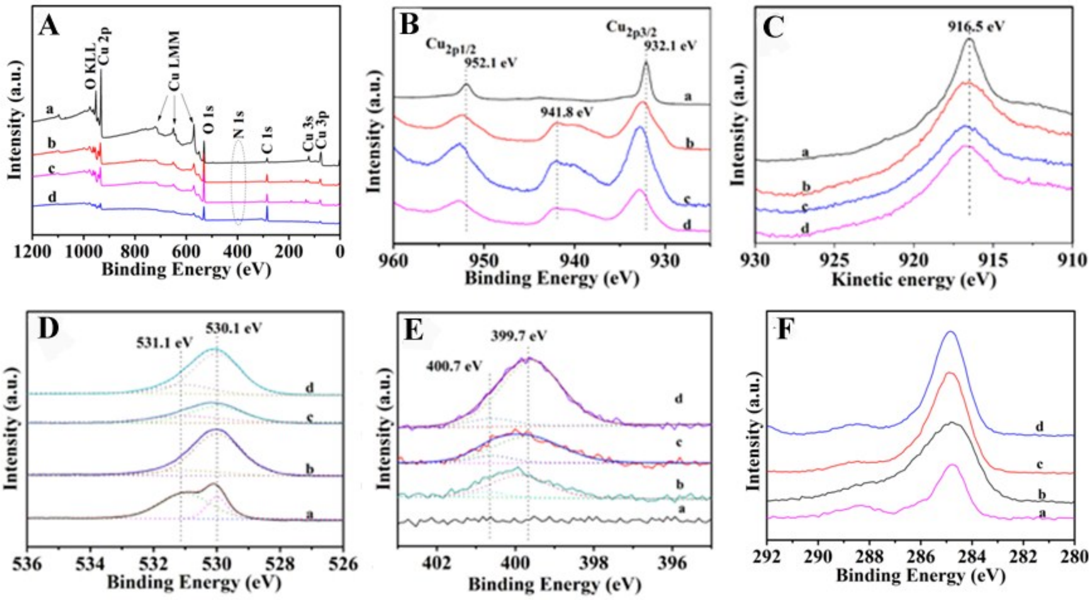

Fig. S4. (A) XPS survey spectrand high-resolution XPS spectra of (B) Cu 2p, (C) Cu LMM, (D) O 1s, (E) N 1s and (F) C 1s. (a to d: Cu_2O/ITO, NIP/ Cu_2O/ITO, MIP (with MC-LR)/Cu_2O/ITO, MIP/Cu_2O/ITO).

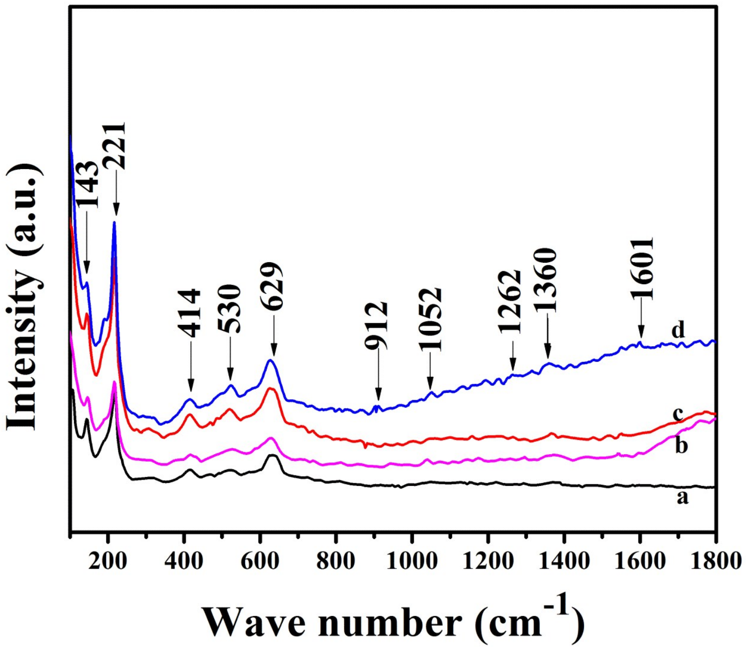

Fig. S5. Raman spectra of different electrode materials. (from a to d: Cu_2O/ITO, NIP/ Cu_2O/ITO, MIP (with MC-LR)/Cu_2O/ITO, MIP/Cu_2O/ITO).

The Raman spectra of different modified electrode materials were shown in Fig. S4. All samples showed Raman shifts at 98, 144, 216, 308, 414, 521 and 629 cm^{-1}, respectively. The strongest peak at 216 cm^{-1} was assigned to the second-order Raman-allowed mode $2\Gamma_{12}^{-}$of the Cu_2O crystals, which demonstrated the high structural quality of the synthesized samples.[2] The second intense Raman peak at 98 cm^{-1} was attributed to the silence mode Γ_{25}^{-}[3] and the peak at 144 cm^{-1} belonged to the infrared active mode of Γ_{15}^{-1}.[4] Three relatively weak peaks at 414 cm^{-1}, 521 cm^{-1}, and 629 cm^{-1} were assigned to four phonon mode (3 Γ_{12}^{-}+ Γ_{25}^{-}), Raman-allowed mode Γ_{25}^{+} and red-allowed mode $\Gamma_{15}^{(2)}$ in Cu_2O, respectively.[5] In addition, the peak at 308 cm^{-1} corresponded to the second-order overtone mode $2\Gamma^{(1)}{}_{15-}$.[4] The characteristic peaks of CuO under the same experimental conditions at 298, 330 and 602 cm^{-1} could not be detected and therefore suggests that the Cu_2O film is free of this contaminant.[2] After electropolymerization of PPy, all Raman peaks in the range of 50-700 cm^{-1} almost didn't change.[6] However, from the b to d curves , PPy base bands were located at 1601 cm^{-1} (C=C stretching in the pyrrole ring),[7] 1360 cm^{-1} (ring-stretching mode of PPy),[8] 1262 cm^{-1} (anti-symmetrical C-H in plane deformation), 1052 cm^{-1} (symmetrical C-H in plane deformation), 912 cm^{-1} (C-H out of the plane deformation).[9] The peaks in the range of 800-1800 cm^{-1} was very weak, which implied the amount of molecular imprinted PPy was low.

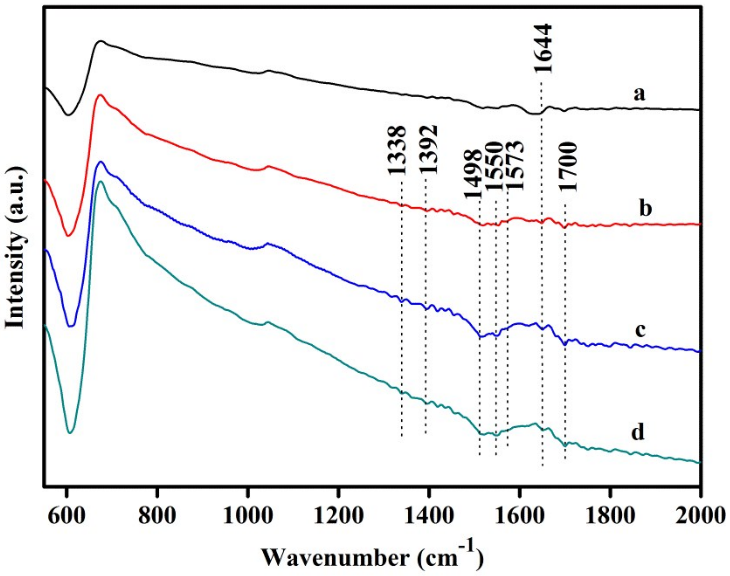

Fig. S6. FTIR spectra of different electrode materials. (from a to d: Cu_2O/ITO, NIP/ Cu_2O/ITO, MIP (with MC-LR)/Cu_2O/ITO, MIP/Cu_2O/ITO).

The Fourier transform infrared (FTIR) spectra of different modified electrode materials were shown in Fig. S6. The intense absorption band at 609 cm^{-1} was assigned to the characteristic Cu-O stretching vibration in the Cu_2O phase.[10] The band at 1630 cm^{-1} was respectively caused by bending vibration of surface O-H bond of adsorbed H_2O. The peaks at 1550 cm^{-1} and 1498 cm^{-1} were correspond to the anti-symmetric and symmetric stretching vibration of C=C in pyrrole rings,[11, 12] while the peaks at 1338 cm^{-1} were due to C-N stretching vibration of pyrrole rings. These results indicated that the PPy was formed successfully on the surface of Cu_2O films. After the MIP modification with MC-LR, the characteristic peaks centered at 1647 cm^{-1} and 1573 cm^{-1} appeared which could be ascribed to bending vibration of -CO-NH-, and -N-H bonds, respectively.[13] The band at 1392 cm^{-1} corresponded to the COO^- asymmetric stretching vibration,[14] while the band at 1700 cm^{-1} was attributed to C=O stretching vibration.[15] After removing the template molecule (MC-LR), the intensities of these three peaks decreased obviously, which implied the recognition sites for MC-LR were successfully constructed on the PPy films.

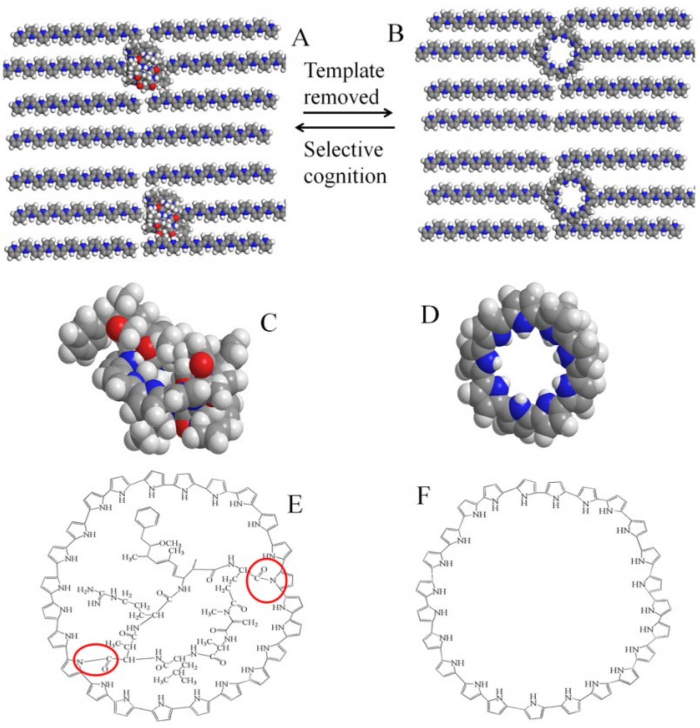

Scheme S1 Schematic diagram of MC-LR recognition mechanism

Table S1 Atomic percent of Cu_2O/ITO, NIP/Cu_2O/ITO, MIP (with MC-LR)/Cu_2O/ITO, MIP/Cu_2O/ITO electrodes

Samples	Atomic%			
	C1s	N1s	O1s	Cu 2p
Cu_2O/ITO	44.52	-	41.4	14.07
NIP/Cu_2O/ITO	37.32	1.03	49.33	15.92
MIP (with MC-LR)/Cu_2O/ITO	48.50	1.36	40.08	10.07
MIP/Cu_2O/ITO	40.77	0.69	45.78	12.76

Table S2. Comparison of the present and other reported methods for the MC-LR detection.

Methods	Analytical range	LOD	Ref.
Fluorescent aptasensor	0.4 - 1200 nM	138 pM	16
Electrochemical immunosensor	0.0025 - 5 ug·L^{-1}	1.68 ng·L^{-1}	17
ECL biosensor	0.1 - 1000 pM	0.03 pM	18
Colorimetric detection	0.1 - 250 nM	0.05 nM	19
Chemiluminescence immunoassay	0.02 - 200 μg·L^{-1}	0.006 ug·L^{-1}	20
This work	0.001 - 10 μg·L^{-1}	0.23 ng·L^{-1}	

Table S3. Comparison of the present and other PEC sensors for the MC-LR detection.

Materials and method	Analytical range	LOD	Re.
MIP@TiO$_2$ NTs	0.5 - 100 μg·L^{-1}	0.1 μg·L^{-1}	21
CdS/graphene immunoassay	0.01 - 25 μg·L^{-1}	0.010 μg·L^{-1}	22
GQD/silicon NW immunosensor	0.1 - 10 μg·L^{-1}	0.055 μg·L^{-1}	23
BiOBr nanoflakes/N-GR aptasensor	1.0 pM - 100 nM	0.03 pM	24
GR@TiO$_2$ NTs aptasensor	1.0 - 500 fM	0.5 fM	25
MI-TiO$_2$@CNTs	1.0 pM - 3.0 nM	0.4 pM	26
CdS/TiO$_2$ NRAs-Fe$_3$O$_4$@PDA immunosensor	0.005 - 500 μg·L^{-1}	0.001μg·L^{-1}	27
CdS/B-TiO$_2$ immunosensor	0.001 - 100 μg·L^{-1}	0.7 ng·L^{-1}	28
This work	0.001 - 10 μg·L^{-1}	0.23 ng·L^{-1}	

Reference

1. J. Chen, C. Shu, N. Wang, J. Feng, H. Ma and W. Yan, *J. Colloid Interf. Sci.*, 2017, **495**, 44-52.
2. S. Shyamal, P. Hajra, H. Mandal, J. K. Singh, A. K. Satpati, S. Pande and C. Bhattacharya, *ACS Appl. Mater. Interfaces*, 2015, **7**, 18344-18352.
3. H. Zhang, D. Zhang, L. Guo, R. Zhang, P. Yin and R. Wang, *J. Nanosci. Nanotechnol.*, 2008, **8**, 6332-6337.
4. Y. Mao, J. He, X. Sun, W. Li, X. Lu, J. Gan, Z. Liu, Li Gongb, J. Chen, P. Liu and Y. Tong, *Electrochim. Acta*, 2012, **62**, 1-7.
5. P. Wang, Y. H. Ng and R. Amal, *Nanoscale*, 2013, **5**, 2952-2958.
6. E. Kecsenovity, B. Endrődi, P. S. Tóth, Y. Zou, R. A. W. Dryfe, K. Rajeshwar and C. Janáky, *J. Am. Chem. Soc.*, 2017, **139**, 6682-6692.
7. J. Kopecká, M. Mrlík, R. Olejník, D. Kopecký, M. Vrňata, J. Prokeš, P. Bober, Z. Morávková, M. Trchová and J. Stejskal, *Sensors*, 2016, **16**, 1917.
8. G. Han and G. Shi, *J. Appl. Polym. Sci.*, 2007, **103**, 1490-1494.
9. I. Chikouche, A. Sahari, A. Zouaoui and S. Tingry, *Can. J. Chem. Eng.*, 2015, **93**, 1076-1080.
10. G. Papadimitropoulos, N. Vourdas, V. E. Vamvakas and D. Davazoglou, *Thin Solid Films*, 2006, **515**, 2428-2432.
11. Z. Fan, J. Zhu, X. Sun, Z. Cheng, Y. Liu and Y. Wang, *ACS Appl. Mater. Interfaces*, 2017, **9**, 21763-21772.
12. J. Jun, J. S. Lee, D. H. Shin, J. Oh, W. Kim, W. Na and J. Jang, *J. Mater. Chem. A*, 2017, **5**, 17335–17340.
13. S.-D. Pan, X.-H. Chen, X.-P. Li, M.-Q. Cai, H.-Y. Shen, Y.-G. Zhao and M.-C. Jin, *J. Mater. Chem. A*, 2015, **3**, 23042–23052.
14. Y. Chen, X. Zhang, Q. Liu, X. Wang, L. Xu and Z. Zhang, *J. Hazard. Mater.*, 2015, **299**, 325-332.
15. W. Teng, Z. Wu, J. Fan, W.-x. Zhang and D. Zhao, *J. Mater. Chem. A*, 2015, **3**, 19168–19176.
16. S. M. Taghdisi, N. M. Danesh, M. Ramezani, N. Ghows, S. A. Mousavi Shaegh and K. Abnous, *Talanta*, 2017, **166**, 187 - 192.

17. J. Zhang, Y. Sun, H. Dong, X. Zhang, W. Wang and Z. Chen, *Sensor. Actuat. B-Chem.*, 2016, **233**, 624 - 632.
18. X. Du, D. Jiang, N. Hao, J. Qian, L. Dai, L. Zhou, J. Hu and K. Wang, *Anal. Chem.*, 2016, **88**, 9622-9629.
19. F. Wang, S. Liu, M. Lin, X. Chen, S. Lin, X. Du, H. Li, H. Ye, B. Qiu, Z. Lin, L. Guo and G. Chen, *Biosen. Bioelectron.*, 2015, **68**, 475 - 480.
20. J. Lu, W. Wei, L. Yin, Y. Pu and S. Liu, *Analyst*, 2013, **138**, 1483-1489.
21. K. Chen, M. Liu, G. Zhao, H. Shi, L. Fan and S. Zhao, *Environ. Sci. Technol.*, 2012, **46**, 11955-11961.
22. J. Tian, H. Zhao, H. Zhao and X. Quan, *Microchim. Acta*, 2012, **179**, 163 - 170.
23. J. Tian, H. Zhao, X. Quan, Y. Zhang, H. Yu and S. Chen, *Sensor. Actuat. B-Chem.*, 2014, **196**, 532-538.
24. X. Du, D. Jiang, L. Dai, L. Zhou, N. Hao, J. Qian, B. Qiu and K. Wang, *Biosen. Bioelectron.*, 2016, **81**, 242-248.
25. M. Liu, J. Yu, X. Ding and G. Zhao, *Electroanalysis*, 2016, **28**, 161-168.
26. M. Liu, X. Ding, Q. Yang, Y. Wang, G. Zhao and N. Yang, *J. Hazard. Mater.*, 2017, **331**, 309-320.
27. J. Wei, A. Qileng, Y. Yan, H. Lei, S. Zhang, W. Liu and Y. Liu, *Anal. Chim. Acta*, 2017, **994**, 82-91.
28. A. Qileng, Y. Cai, J. Wei, H. Lei, W. Liu, S. Zhang and Y. Liu, *Sensor. Actuat. B-Chem.*, 2018, **254**, 727-735.